Effects of the molar mass of the matrix on electrical properties, structure and morphology of plasticized PANI–PMMA blends

2008 J. Phys.: Condens. Matter 20 125221

(http://iopscience.iop.org/0953-8984/20/12/125221)

J. Phys.: Condens. Matter **20** (2008) 125221 (9pp) doi:10.1088/0953-8984/20/12/125221

Effects of the molar mass of the matrix on electrical properties, structure and morphology of plasticized PANI–PMMA blends

Fethi Gmati, Arbi Fattoum, Nadra Bohli and Abdellatif Belhadj Mohamed

Laboratory of Nano Materials, and Systems for Energy (LaNSE), Centre of Research and Technology of Energy (CRTEn), Technopole of Borj Cedria, Hammam Lif 2050, Tunisia

E-mail: gmati_fethi@yahoo.fr

Received 28 December 2007, in final form 11 February 2008
Published 3 March 2008
Online at stacks.iop.org/JPhysCM/20/125221

Abstract

The effects of the molar mass of polymethylmethacrylate (PMMA) on electrical, structural and morphological properties of conductive polyaniline–polymethylmethacrylate blends have been studied. We have plasticized the PMMA matrix by using dioctyl phthalate (DioPh). Three different molar masses of PMMA, 15 000, 120 000 and 350 000 g mol^{-1}, have been used. The x-ray diffraction analysis showed amorphous structure for all our studied PANI–PMMA blend films. The SEM micrographs showed more aggregation with the lowest molar mass of PMMA matrix. The direct current (dc) and alternating current (ac) electrical conductivities have been investigated in the temperature range 20–300 K and frequency range 7–1 $\times$ 10^8 Hz. The results of this study indicate an increase of the conductivity when the molar mass of PMMA decreases. With the lowest molar mass of PMMA (15 000 g mol^{-1}), we obtained the lowest percolation threshold ($p_c \approx 0.3\%$). The dc conductivity is governed by Mott's three-dimensional variable range hopping (3D VRH) model; different Mott's parameters have been evaluated. At high frequencies, the ac conductivity follows the power law $\sigma(\omega, T) = A(T)\omega^{s(T,\omega)}$, which is characteristic for charge transport in disordered materials by hopping or tunnelling processes. The observed decrease in the frequency exponent s with increasing temperature suggests that the correlated barrier hopping (CBH) model best describes the ac conduction mechanism. All our blends are well described by the scaling law $\sigma(\omega)/\sigma_{dc} = 1 + (\omega/\omega_c)^n$ with $n \approx 0.51$–0.52.

1. Introduction

The combination of conducting polymers with insulating polymer matrixes has attracted the interest of several researchers during the last few years, due to their significant importance in technological applications in different fields including solar cells, optoelectronics, electromagnetic shielding, microwave absorption, conducting membrane materials and conducting glues [1]. In general, the matrix assures good mechanical properties, environmental stability and easy processability of the blend, while electrical conductivity results from the inserted conducting polymer in the matrix [1]. Besides polypyrrole and polythiophene and their derivatives, polyaniline (PANI) is one of the most commonly used conducting polymers, due to its combination of high electrical conductivity, environmental stability and facility of synthesis [1–5]. For the preparation of PANI blends, several methods have been developed; known methods may be essentially reduced to two distinct groups: the synthesis methods based on aniline polymerization in the presence or inside the polymer matrix, and the blending methods which consist of mixing previously prepared PANI with a polymer matrix [1–7].

Earlier studies concerning PANI blends made with different insulating matrixes showed that charge transport, morphology and structure depend strongly on many parameters, such as the matrix itself, the average size and the network structure of PANI particles in the blend, the nature of dopant, the plasticizer and the preparation method. In this

field, several polymer matrixes were used to obtain PANI blends; we cite polymethylmethacrylate (PMMA) [2–7], cellulose acetate (CA) [8–11], polyvinylchloride (PVC) [12–14], polystyrene (PS) [15], styrene–butadiene–styrene (SBS) [16], polyurethane (PU) [17], polyethylene terephthalate (PET) [18] and polyvinyl alcohol (PVA) [19]. To explain the charge transport in conducting polymer blends, various models were adopted. The electrical conductivity in such materials is assigned to phonon assisted hopping or tunnelling of charge carriers (solitons, polarons and bipolarons) between electronic localized states randomly distributed. In general, the dc conductivity measurements must be completed by ac measurements to obtain rich additional information about the conduction mechanism that dc measurements alone do not provide [19–41]. In several works, the ac conduction mechanism in conducting polymer blends has been studied [19, 20, 29, 33, 39, 42–46]. In PANI–CA [8–11] and PANI–PVA [19] blends, the dc conductivity is well described by the generalized Mott's variable range hopping (VRH) model. Reghu *et al* showed in their works [2–5] that dc conductivity of PANI–PMMA blends, above the percolation threshold, is well described by the generalized Mott's variable range hopping (VRH) model with an exponent which increases by increasing the weight fraction of PANI. Dey *et al* [31] showed that dc conductivity of PANI–TiO_2 follows the three-dimensional VRH model. However, there exist other PANI blends where the charge transport is described by the quasi-one-dimensional VRH model [47]. Kaiser *et al* [14] showed that dc conductivity of PANI–PMMA blends is described in the framework of a heterogeneous picture by the charging energy limited tunnelling (CELT) model [15, 35–38]. It was found that other PANI blends such as PANI–PET [18], PANI–PS [15] are also well described by the CELT model. Although the important role of different insulating matrixes in the modification of conduction mechanisms of conducting polymer blends has been discussed, the effect of the molar mass of the matrix is generally not taken into account. The use of various polymeric matrixes having the same monomer unit but differing in their chain length is of fundamental interest to study the influence of this parameter on electrical and structural properties of the obtained blend.

The aim of the present work is to study the effect of the molar mass of the PMMA matrix on the electrical properties (conductivity, percolation threshold, dc and ac conduction mechanisms), structure and morphology of plasticized PANI–PMMA blend films, prepared at various weight fractions of polyaniline.

2. Experimental techniques

2.1. Sample preparation

Conducting polyaniline (PANIPLAST COX-DCAA, France), dispersed in dichloroacetic acid (DCAA), was mixed in an appropriate ratio with solutions of polymethylmethacrylate (PMMA) (Aldrich) plasticized with dioctyl phthalate (DioPh) (Aldrich) (35% with respect to PMMA mass) using the same solvent, DCAA. We have used different molar masses for PMMA: 15 000, 120 000 and 350 000 g mol^{-1}, denoted respectively PMMA1, PMMA2 and PMMA3. The blend solution was magnetically stirred for 48 h, and then cast onto glass substrates to obtain thin films. After drying at 50 °C for 72 h, the film was peeled to obtain a free standing film for measurements. We have determined the thickness of the cast films by using scanning electron microscopy (SEM) observations. Values were found to be between 60 and 70 μm.

2.2. Characterization and techniques

X-ray diffraction (XRD) measurements were carried out by using a PANalytical/X'Pert Pro MPD x-ray diffractometer using cobalt radiation ($\lambda = 1.79$ Å) in the 2θ range of 0°–40°. Ultraviolet–visible (UV–vis) spectra were obtained on a Shimadzu 3100 spectrophotometer. The scanning electron microscopy (SEM) micrographs were obtained from a Philips XL 30 scanning electron microscope operating at 20 kV. The impedance $Z(\omega) = Z'(\omega) + jZ''(\omega)$ of the blend films was measured by using an HP 4192A LF impedance analyser in the frequency range of 7–10^8 Hz by adopting coplanar geometry electrical contacts [42]. The temperature of the film was varied between 20 and 300 K. For this, a closed cycle helium cryostat was used to lower the temperature, which was controlled by a Lakeshore 331 controller. The sample is modelled by an RC parallel circuit [28, 30, 48]. The relative complex permittivity of the material is defined by $\varepsilon_r^*(\omega) = \varepsilon_r'(\omega) - i\varepsilon_r''(\omega)$, where $\varepsilon_r''(\omega)$ describes the global loss factor in the material and is given by $\varepsilon_r''(\omega) = \frac{1}{C_0\omega}\frac{Z'}{Z'^2+Z''^2}$, where C_0 is the capacitance with a free space between the electrodes and $\omega = 2\pi F$ is the angular frequency of the applied electric field. The ac conductivity $\sigma(\omega)$ was calculated from the global loss factor according to the following relation: $\sigma(\omega) = \omega\varepsilon_0\varepsilon_r''(\omega)$, where ε_0 is the permittivity of vacuum.

The dc conductivity measurements were made using an Agilent Multimeter 34401A. The bulk resistance R of the samples was determined by employing the formula $\sigma_{dc} = \frac{1}{R}\frac{L}{d\cdot l}$, where L is the distance between the contacts and d and l are the thickness and the length of the film, respectively.

3. Results and discussion

3.1. UV–vis absorption study

The UV–vis absorption spectra of the conducting PANI and the PANI–PMMA blends at 4% PANI weight fraction are presented in figure 1. Two absorption bands at 285 nm and 443 nm are recognized in the PANI spectra and assigned respectively to π–π^* and polaron transitions [5, 49, 50]. A broad band around 1200 nm is also observed. This band is characteristic of polaron delocalization and is called the free carrier tail [7, 51]. These absorption bands also appear in the blend spectra, independently of the molar mass of the PMMA matrix. This fact supports that PANI conserves its initial electronic structure after being embedded into the PMMA matrix. Our results are similar to those obtained for self-assembled nanofibres of polyaniline blended with PMMA (100 000 g mol^{-1}) [6].

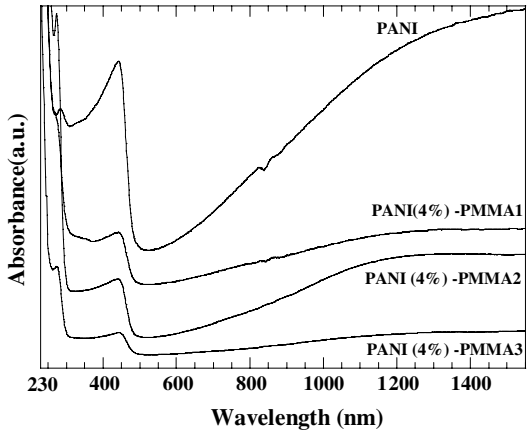

Figure 1. UV–vis spectra of PANI, PANI (4%)–PMMA1, PANI (4%)–PMMA2 and PANI (4%)–PMMA3 blends.

3.2. Sample morphology

The (SEM) micrographs of PANI–PMMA blend films at 10% PANI weight fraction are shown in figure 2. It is visible that blends show aggregated structure. The granular particles can be attributed to the PANI clusters embedded in the PMMA matrix [5, 13]. The effect of the molar mass of the PMMA matrix can be observed in the surface morphology of the blends. In fact, PANI–PMMA1 shows more aggregation than PANI–PMMA3.

3.3. X-ray diffraction studies

Figure 3 shows x-ray diffraction patterns recorded for unblended PANI, PMMA and PANI–PMMA blends at 4%. We note the semi-crystalline structure of the conducting PANI films, characterized by the presence of the diffraction peaks at $2\theta = 17.8°$, $23.33°$, $29.6°$ and $31.4°$. For the PMMA matrix alone, the x-ray patterns show broad peaks around 15.5° and 35.5°, indicating amorphous structure. The PANI–PMMA blend x-ray patterns are characterized by the absence of the PANI peaks and the broadening of the PMMA ones, indicating amorphous structure of the blend. This amorphous structure may be attributed to the formation of a network in which PANI and PMMA chains are interpenetrated [5].

3.4. Conductivity studies

The figure 4 shows that the room dc conductivity of the PANI–PMMA blends is best described by the percolation scaling law [52]:

$$\sigma(p) = c|p - p_c|^t \qquad (1)$$

where c is a constant, t the universal exponent and p_c the percolation threshold. The best fitted values of t and p_c are shown in table 1. For each PANI weight fraction, the conductivity increases when the molar mass of PMMA decreases. In addition, the percolation threshold p_c decreases when the molar mass of the PMMA matrix decreases. In fact, during the liquid–liquid phase separation process, the mobility of the macromolecules becomes greater when the molar mass decreases. This enhances the diffusion of PANI chains between the PMMA ones. As a result, the blend more closely approaches the morphology associated with the minimum energy morphology of the PANI self-assembled network [3].

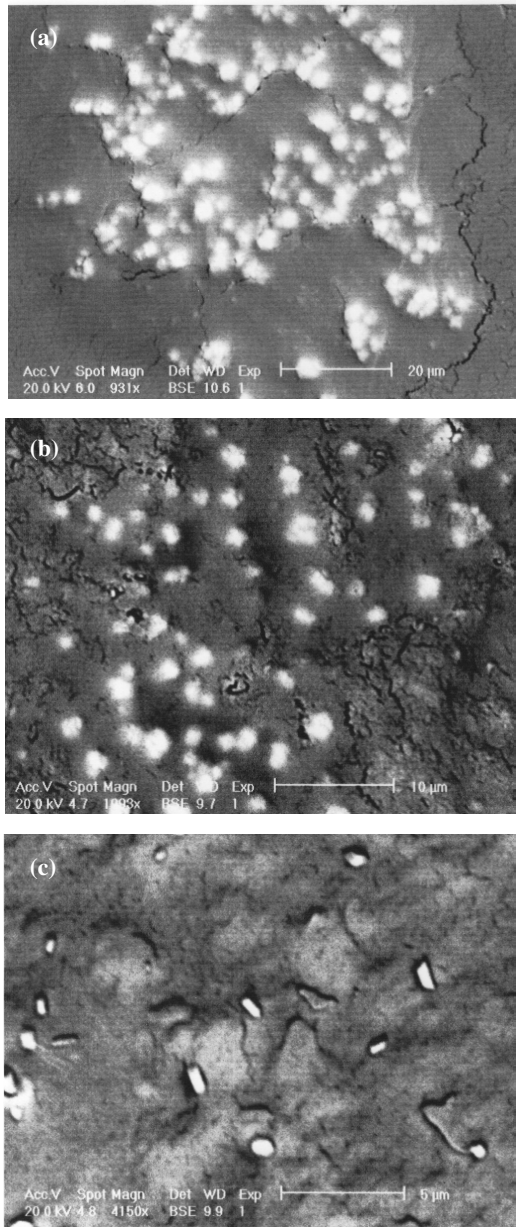

Figure 2. Scanning electron micrographs of (a) PANI (10%)–PMMA1, (b) PANI (10%)–PMMA2 and (c) PANI (10%)–PMMA3 blends.

Table 1. Values of the percolation threshold p_c and exponent t for various PANI–PMMA blends.

Samples	p_c	Exponent t
PANI–PMMA1	0.003	2.1724
PANI–PMMA2	0.005	2.3772
PANI–PMMA3	0.010	2.4839

In order to study the effect of the matrix molar mass on the dc conduction mechanism in our blends, we present in figure 5

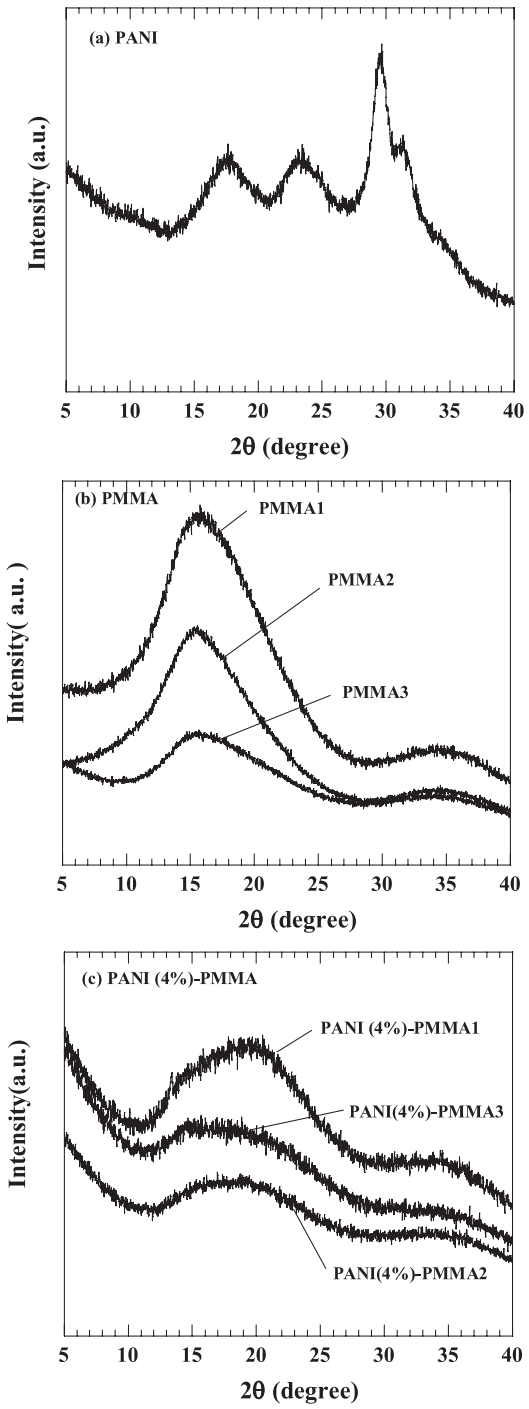

Figure 3. X-ray diffraction patterns of (a) conducting PANI, (b) PMMA matrixes and (c) various PANI (4%)–PMMA blends.

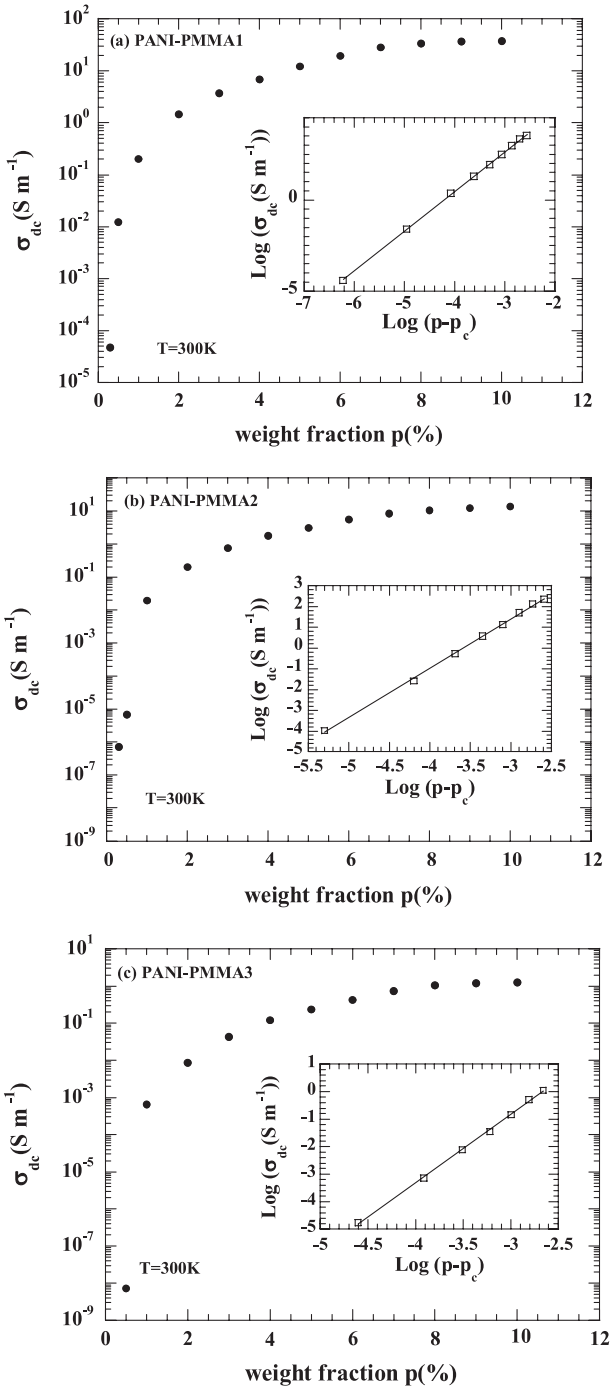

Figure 4. Variation of dc conductivity versus the weight fraction of PANI for (a) PANI–PMMA1, (b) PANI–PMMA2 and (c) PANI–PMMA3 blends. Insets show the percolation scaling law, $\log \sigma_{dc}$ versus $\log (p–p_c)$. The values of p_c are listed in table 1.

the variation of σ_{dc} versus temperature for various PANI (10%)–PMMA blends. The observed increase in σ_{dc} with temperature indicates semiconductor behaviour [4, 19, 29, 53]. The effect of temperature on conductivity is similar for all other compositions exceeding p_c. To determine the best compatible charge transport mechanism, we have analysed the measured dc conductivity data by several conduction models [14, 20, 37, 38]. The best fits were obtained with the 3D VRH conduction model. In this model, when the interaction between charge carriers is neglected, the dc conductivity is given by [20]

$$\sigma_{dc} = B\,(T_0/T)^{1/2}\,\exp[-(T_0/T)^{1/4}] \qquad (2)$$

where B is a constant given by [20]

$$B = N(E_F)\,e^2 \nu_{ph} \frac{9}{64\alpha^2}, \qquad (3)$$

Table 2. Values of dc conductivity (σ_{dc}), Mott's parameters, characteristic temperature (T_0), density of states at the Fermi level ($N(E_F)$), average hopping distance (R_{hop}), average hopping energy (W_{hop}), $R\alpha$ at 300 and 100 K for PANI (10%)–PMMA blends.

Samples	σ_{dc} (S m^{-1}) 300 K	T_0 (K)	$N(E_F)$ (eV^{-1} cm^{-3})	R_{hop} (300 K) (nm)	W_{hop} (300 K) (meV)	R_{hop} (100 K) (nm)	W_{hop} (100 K) (meV)	$R_{hop}\alpha$ 300 K	$R_{hop}\alpha$ 100 K
PANI (10%)–PMMA1	37.571	1.39×10^6	1.14×10^{20}	3.4	53.3	4.48	23.3	3.1	4.1
PANI (10%)–PMMA2	13.593	1.62×10^7	9.77×10^{18}	6.3	97.73	8.27	43.20	5.73	7.52
PANI (10%)–PMMA3	1.2613	3.25×10^8	4.86×10^{17}	13.31	208.35	17.51	91.5	12.1	15.92

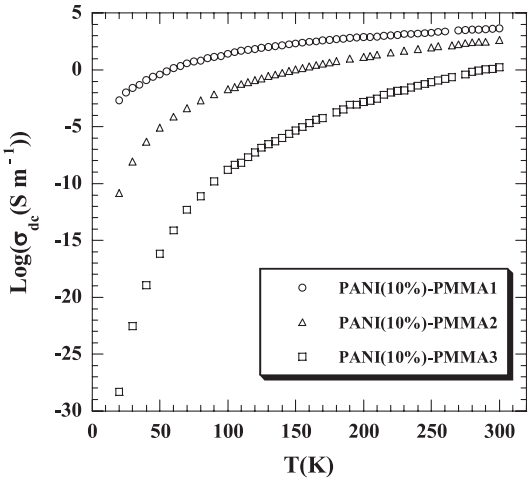

Figure 5. Variation of dc conductivity (σ_{dc}) ($\log \sigma_{dc}$) versus temperature for PANI (10%)–PMMA1, PANI (10%)–PMMA2 and PANI (10%)–PMMA3 blends.

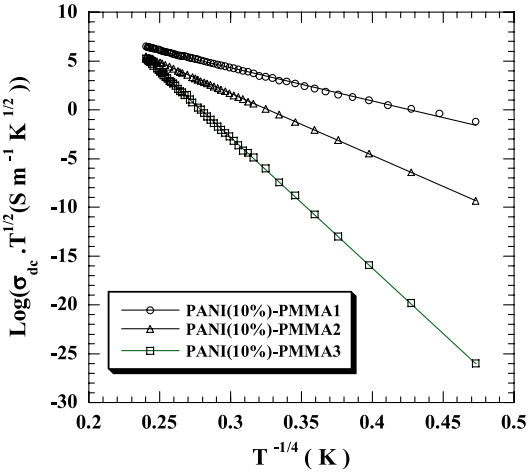

Figure 6. Variation of the dc conductivity ($\log \sigma_{dc} T^{1/2}$) versus temperature ($T^{-1/4}$) for PANI (10%)–PMMA1, PANI (10%)–PMMA2 and PANI (10%)–PMMA3 blends (the solid lines are fitted curves to the 3D VRH model) in the temperature range 20–300 K.

where $N(E_F)$ is the density of states at the Fermi level, e is the elementary charge (1.6×10^{-19} C), ν_{ph} is the phonon frequency ($\approx 10^{13}$ Hz), $1/\alpha$ is the decay length of the localized wavefunction. T_0 is the characteristic temperature of Mott, given by [20]

$$T_0 \cong 18.11 \frac{\alpha^3}{N(E_F)\, k_B} \tag{4}$$

k_B is the Boltzman constant (1.38×10^{-23} J K^{-1}).

The average hopping distance R_{hop} and the average hopping energy W_{hop} are given respectively by [20]

$$R_{hop} = \left[\frac{9}{8\,\alpha\,\pi\, N(E_F) k_B\, T} \right]^{1/4} \tag{5}$$

$$W_{hop} = \frac{3}{4\pi N(E_F) R_{hop}^3}. \tag{6}$$

We present in figure 6, $\log(\sigma_{dc} T^{1/2})$ versus $T^{-1/4}$ for the same samples of PANI (10%)–PMMA. The linear behaviour of the plots indicates that the 3D VRH mechanism is appropriate to describe the temperature dependence of conductivity. Different Mott parameters such as T_0, $N(E_F)$, R_{hop} and W_{hop} have been evaluated at 300 and 100 K using equations (4)–(6) and listed in table 2; α^{-1} was assumed to be 1.1 nm [28, 54]. It is clear from table 2 that the density of localized states $N(E_F)$ decreases when the molar mass of the PMMA matrix is increased. On the other hand, the average hopping distance R_{hop}, the average hopping energy W_{hop} and the size of the hopping barrier T_0 decrease when the molar mass of the PMMA matrix is decreased; this enhances hops between PANI chains and leads to an increase in conductivity. In fact, with greater molar mass of PMMA matrix, i.e. with longer chain, the insulating barrier between PANI chains becomes larger and the hop probability of the charge carriers is reduced, which decreases the conductivity of the sample. This result is compatible with the SEM micrographs showing best connectivity between the conducting chains with lowest molar mass of PMMA.

Our results are consistent with Mott's requirements: $R_{hop}\alpha > 1$ and $W_{hop} > k_B T$. $R_{hop}\alpha$, called the degree of localization [28], is found to be $\approx$3.1 for PANI–PMMA1 and 12.1 for PANI–PMMA3 at $T = 300$ K. This indicates that the charge carriers become more localized when the molar mass of PMMA in the blend increases and explains the associated decrease observed in the conductivity. It is also visible from table 2 that, when we decrease temperature, the average hopping energy W_{hop} decreases, and the average hopping distance R_{hop} increases. This supports the idea that when the phonon energy is insufficient (low temperature) carriers will hop larger distances in order to locate sites which are energetically closer than their nearest neighbours [20].

The conductivity in alternative current is plotted in order to obtain additional information about charge transport. We

Table 3. The best fitted values of W_m and τ_{oh} at a fixed frequency and temperature, the calculated hopping distance R_ω and the density of states at the Fermi level $N(E_F)$ at 295 K and the frequency exponent s at 280 K for various PANI(2%)–PMMA blends.

Samples	W_m (eV)	τ_{oh} (s)	$\sigma(\omega)$ (S m^{-1}) $\omega = 4.27 \times 10^6$ (rad s^{-1}), $T = 295$ K	$N(E_F)$ (eV^{-1} cm^{-3})	R_ω (10^{-3} nm)	Exponent s $T = 280$ K
PANI (2%)–PMMA1	0.11	0.407×10^{-4}	4.48×10^{-1}	8×10^{30}	1.6	0.44
PANI (2%)–PMMA2	0.15	1.41×10^{-4}	3.024×10^{-1}	2.23×10^{31}	1.01	0.51
PANI (2%)–PMMA3	0.66	3×10^{-4}	1.35×10^{-1}	5.35×10^{31}	0.3	0.56

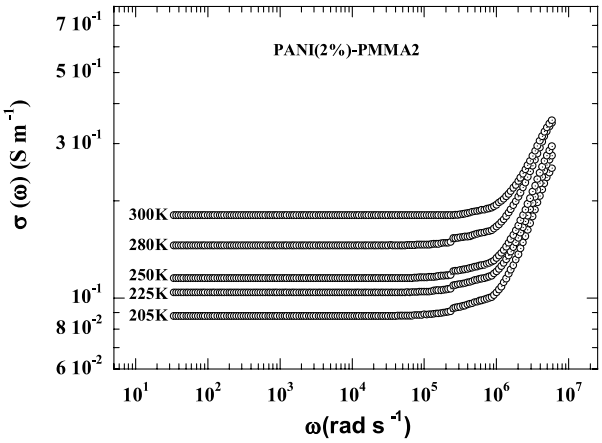

Figure 7. Angular frequency dependence of conductivity ($\log \sigma$ versus $\log \omega$) for PANI (2%)–PMMA2 blend at various temperatures.

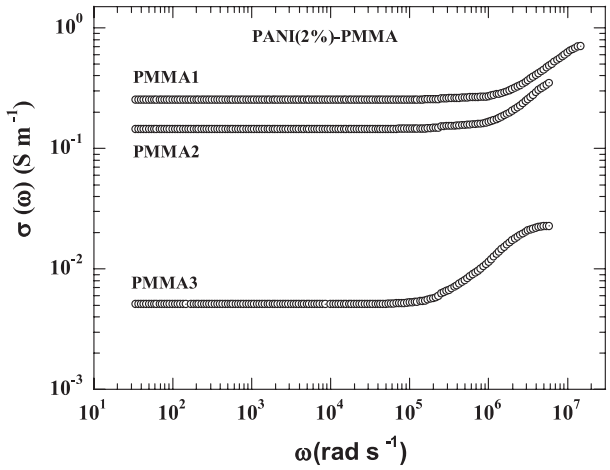

Figure 8. Angular frequency dependence of the conductivity ($\log \sigma$ versus $\log \omega$) for PANI (2%)–PMMA1, PANI (2%)–PMMA2 and PANI (2%)–PMMA3 blends at $T = 280$ K.

present in figure 7 the variation of the conductivity versus frequency at different temperatures for PANI (2%)–PMMA2 blend. In figure 8, we present the frequency dependence of the conductivity at 280 K, for PANI–PMMA1, PANI–PMMA2 and PANI–PMMA3 blends having the same PANI weight fraction. All curves exhibit two distinct regions: at low frequencies a plateau is present, i.e. the conductivity $\sigma(\omega, T)$ maintains a constant value ($\sigma(\omega, T) \approx \sigma_{dc}(T)$) up to a critical angular frequency ω_c, at which the conductivity begin to monotonically increase. At high frequencies ($\omega > \omega_c$), the conductivity follows an apparent power law: $\sigma(\omega, T) \approx \sigma_{ac}(\omega, T) \approx A(T)\omega^{s(\omega,T)}$, where A depends on temperature and the exponent s is frequency and temperature dependent and lies between zero and unity. This behaviour is reproducible for all other compositions. Similar behaviour was observed in various conducting polymers and their composites [10, 11, 19, 26, 28, 31, 40, 41, 48, 55–57], and in other conducting composites [29, 30, 58]. The conductivity is suitably described by the Jonscher's universal power law [59]:

$$\sigma(\omega, T) = \sigma_{dc}(T) + A(T)\,\omega^{s(T,\omega)}. \tag{7}$$

The angular frequency exponent s is determined from the relation [20]

$$s = \frac{\mathrm{d} \ln \sigma_{ac}(\omega)}{\mathrm{d}\, Ln\, \omega}. \tag{8}$$

At a given temperature and fixed frequency range, the exponent s increases when the molar mass of PMMA in the blend increases (table 3). To determine the compatible

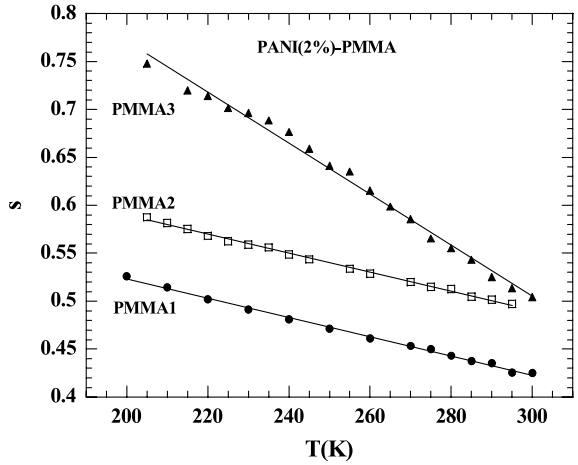

Figure 9. Temperature dependence of the frequency exponent s for PANI (2%)–PMMA1, PANI (2%)–PMMA2 and PANI (2%)–PMMA3 blends (the solid curves are the theoretical values of s according to equation (11)).

mechanism of ac charge transport in our samples, we present in figure 9 the temperature dependence of s for three samples with different molar masses of PMMA at a fixed PANI weight fraction. For each PMMA molar mass, s decreases with increasing temperature. This behaviour is reproducible for all other PANI weight fractions.

The charge transport process in disordered solids in the presence of an alternative field can be described by different

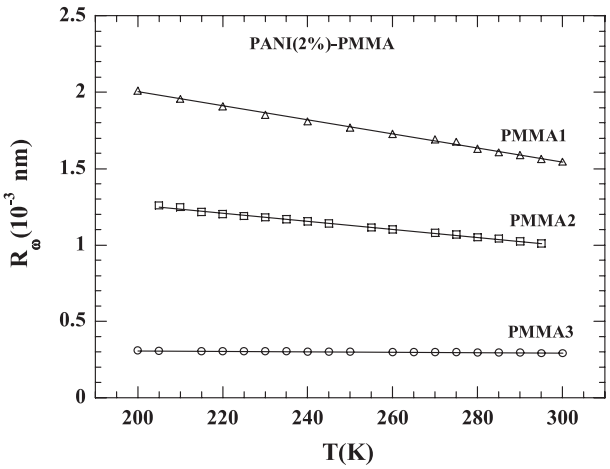

Figure 10. Temperature dependence of the hopping distance R_ω at the frequency $\omega = 4.27 \times 10^6$ rad s^{-1} for various PANI (2%)–PMMA blends at various molar masses of PMMA. The solid curves are the theoretical values of R_ω according to equation (10).

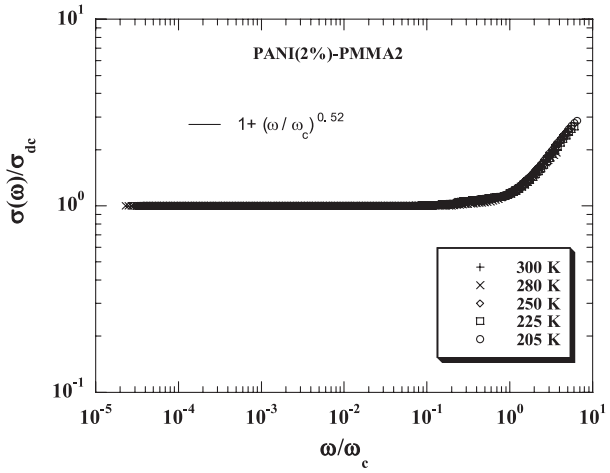

Figure 11. Scaling behaviour of $\sigma(\omega)/\sigma_{dc}$ versus ω/ω_c for the PANI (2%)–PMMA2 blend at various temperatures.

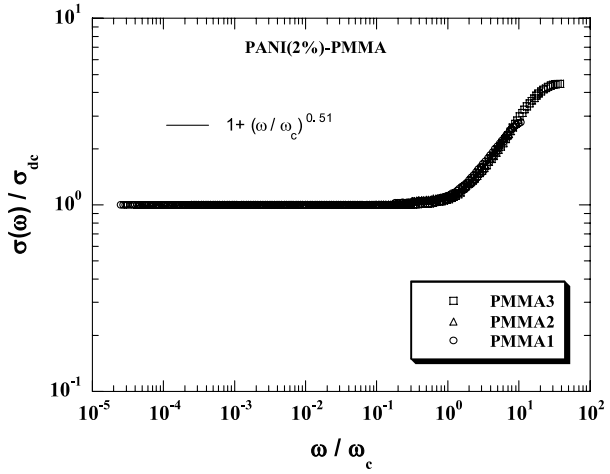

Figure 12. Scaling behaviour of $\sigma(\omega)/\sigma_{dc}$ versus ω/ω_c for PANI(2%)–PMMA blends with various PMMA matrixes at $T = 280$ K.

models such as correlated barrier hopping (CBH) [42], electron tunnelling (quantum mechanical tunnelling (QMT)) [20], small polaron tunnelling, large polaron tunnelling [42] and random free energy barrier (symmetric hopping model) [51]. In the QMT model, the exponent s remains almost equal to 0.8 or increases slightly with increasing temperature [20]; this model may not be applicable to explain the results of the present study. In the small polaron tunnelling model, the exponent s increases with increasing temperature; consequently, this model is also not applicable to explain our results. In the CBH model, s decreases with increasing temperature; this model may be a useful theory to explain the conduction mechanism in our PANI–PMMA blends. This result is in good agreement with that obtained by Dutta *et al* [19] for PANI–polyvinyl alcohol blends and by Dey *et al* [31] for PANI–TiO_2 nanocomposites.

In the CBH model, the ac conductivity is given by [42]

$$\sigma_{ac}(\omega) = \frac{\pi^3}{24} N^2 \varepsilon \varepsilon_0 \omega R_\omega^6 \tag{9}$$

where $N = k_B T N(E_F)$, ε and ε_0 are the dielectric permittivity of the material and free space respectively ($\varepsilon_0 = 8.85 \times 10^{-12}$ F m^{-1}), R_ω is the hopping distance at a particular angular frequency ω and temperature, given by [42]

$$R_\omega = \frac{e^2}{\pi \varepsilon \varepsilon_0} \frac{1}{W_m + k_B T\, Ln(\omega \tau_{oh})}. \tag{10}$$

The frequency exponent in the CBH model is given by [42]

$$s = 1 - \frac{6 k_B T}{W_m + k_B T\, Ln(\omega \tau_{oh})} \tag{11}$$

where W_m is the energy required to remove an electron from one site (activation energy), and τ_{oh} is the relaxation time.

The temperature dependence of R_ω at the angular frequency ($\omega = 4.2 \times 10^6$ rad s^{-1}) for our PANI–PMMA blends with 2% PANI weight fraction is shown in figure 10. We see that R_ω decreases when temperature increases; this is in good agreement with the theoretical prediction of the CBH model. The best fitted values of W_m, τ_{oh}, R_ω and $N(E_F)$ at $\omega = 4.2 \times 10^6$ rad s^{-1} and $T = 295$ K are listed in table 3. It is clear that R_ω becomes shorter when the molar mass of PMMA increases, which is another argument in favour of the CBH model that predicts the decrease of conductivity when the hopping distance decreases. The behaviour of R_ω and $N(E_F)$ is similar to that obtained by Dey *et al* [31] for PANI-TiO_2 nanocomposites. Also, from table 3, when the molar mass of PMMA increases the activation energy W_m increases. i.e. the electron requires more energy to hop from one site to another, which explains the decrease of the ac conductivity with the increase of the molar mass of PMMA.

We present in figure 11 the scaled conductivity $\sigma(\omega)/\sigma_{dc}$ as a function of the scaled frequency ω/ω_c for the PANI (2%)–PMMA2 blend at various temperatures. We present in figure 12 the scaled conductivity for PANI (2%)–PMMA blends with different molar masses of PMMA at 280 K. The scaling

behaviour of the ac conductivity $\sigma(\omega)$ of various conducting polymers and their blends [11, 19, 29, 40, 56] can be described by the following relation [59]:

$$\frac{\sigma(\omega, T)}{\sigma_{dc}} = 1 + (\omega/\omega_c)^n \qquad (12)$$

where n is a constant and ω_c is the characteristic angular frequency defined above in the text. In this scaling law, the exponent n lies between zero and unity. We found that the scaled conductivity of all our blends, as a function of the scaled frequency, follows a muster curve represented by equation (12), with an exponent $n \approx 0.51$–0.52 independently of the PMMA molar mass.

4. Conclusion

Free standing blend films of doped polyaniline (PANI) and polymethylmethacrylate (PMMA) plasticized with dioctyl phthalate (DioPh) have been obtained by using the simple co-dissolution method. The x-ray analysis showed an amorphous structure independently of the molar mass of the used PMMA matrix. The results of the present study suggest that microscopic parameters of charge transport in dc and ac fields depend on the molar mass of the PMMA matrix used in the synthesis of our PANI–PMMA blends. When we decrease the molar mass of PMMA the conductivity increases and the percolation threshold decreases. The charge transport in direct current in all our samples is well represented by Mott's 3D VRH model. The evaluated Mott's parameters allowed us to attribute the influence of the molar mass of the matrix on the conductivity.

The ac conductivity in the high frequency range follows the power law $\sigma(\omega, T) = A(T)\omega^{s(T,\omega)}$, in which the exponent s decreases when the temperature increases, suggesting that the correlated barrier hopping (CBH) model best describes the dominant ac conduction mechanism. The evaluated hopping distance R_ω decreases with increasing temperature. R_ω decreases when we increase the molar mass of PMMA while the activation energy W_m is increased. For all the molar masses, the ac conductivity follows the scaling law $\sigma(\omega)/\sigma_{dc} = 1 + (\omega/\omega_c)^n$ with $n \approx 0.51$–0.52.

References

[1] Pud A, Ogurtsov N, Korzhenko A and Shapoval G 2003 *Prog. Polym. Sci.* **28** 1701–53
[2] Yoon C O, Reghu M, Moses D and Hegger A J 1994 *Synth. Met.* **63** 47–52
[3] Reghu M, Yoon C O, Yang C Y, Moses D, Smith P and Hegger A J 1994 *Phys. Rev.* B **50** 13931–41
[4] Yoon C O, Reghu M, Moses D, Cao Y and Hegger A J 1995 *Synth. Met.* **69** 255–8
[5] Yang C Y, Reghu M, Hugger A J and Cao Y 1996 *Synth. Met.* **79** 27–32
[6] Araujo P L B, Araujo E S, Santos R F S and Pacheco A P L 2005 *Microelectron. J.* **36** 1055–7
[7] Olinga T E, Fraysse J, Travers J P, Dufresne A and Pron A 2000 *Macromolecules* **33** 2107–13
[8] Pron A, Zagorska M, Nicolau Y, Genoud F and Nechtschein M 1997 *Synth. Met.* **84** 89–90
[9] Wolter A, Banka E, Genoud F, Pron A and Nechtschein M 1997 *Synth. Met.* **84** 753–4
[10] Planes J, Banka E, Senis R and Pron A 1997 *Synth. Met.* **84** 797–8
[11] Cheguettine Y, Planes J and Banka E 1999 *Synth. Met.* **101** 787–8
[12] Banerjee P and Mandal B M 1995 *Synth. Met.* **74** 257–61
[13] Laska J, Zak K and Pron A 1997 *Synth. Met.* **84** 117–8
[14] Kaiser A B, Subramanian C K, Gilberd P W and Wessling B 1995 *Synth. Met.* **69** 197–200
[15] Jousseaume V, Morsli M, Bonnet A and Lefrant S 1999 *Synth. Met.* **101** 813–4
[16] Leyva M E, Barra G M O and Soares B G 2001 *Synth. Met.* **123** 443–9
[17] Sanjai B, Raghunathan A, Natarajan T S, Rangaragan G, Thomas S, Pravakaran P V and Venkatachalam S 1997 *Phys. Rev.* B **55** 10734
[18] Plester R, Nimtz G and Wessling B 1994 *Phys. Rev.* B **49** 12718
[19] Dutta P, Biswas S, Ghosh M, De S K and Chatterjee S 2001 *Synth. Met.* **122** 455–61
[20] Mott N F and Davis E A 1979 *Electronic Processes in Non Crystalline Materials* (Oxford: Clarendon) pp 157–600
[21] Prigodin V N, Samukhin A N and Epstein A J 2004 *Synth. Met.* **141** 155–64
[22] Singh R, Tandon R P and Chandra S 1993 *J. Phys.: Condens. Matter* **5** 1313–8
[23] Kahol P K, Pinto N J, Berndtsson E J and McCormick B J 1994 *J. Phys.: Condens. Matter* **6** 5631–8
[24] Ghosh M, Meikap A K, Chattopadhyay S K and Chatterjee S 2001 *J. Phys. Chem. Solids* **62** 475–84
[25] Kumar J, Singh R K, Chand S, Kumar V, Rastogi R C and Singh R 2006 *J. Phys. D: Appl. Phys.* **39** 196–202
[26] Singh R, Kumar J, Singh R K, Rastogi R C and Kumar V 2007 *New J. Phys.* **9** 40
[27] Singh R K, Kumar J, Singh R, Kant R, Rastogi R C, Chand S and Kumar V 2006 *New J. Phys.* **6** 112
[28] Gmati F, Fattoum A, Bholi N, Dhaoui W and Mohamed A B 2007 *J. Phys.: Condens. Matter* **19** 326203
[29] Dutta P and De S K 2003 *Synth. Met.* **139** 201–6
[30] Hernandez J A and Kalmouth K P 2001 *J. Phys. D: Appl. Phys.* **34** 1700–11
[31] Dey A, De S, De A and De S K 2004 *Nanotechnology* **15** 1277–83
[32] Dallas P, Moutis N, Devlin E, Niarchos D and Petridis D 2006 *Nanotechnology* **17** 5019–26
[33] Gmati F, Fattoum A, Mohamed A B, Zangar H, Outzourit A and Achour M S 2007 *Phys. Chem. News* **36** 152–5
[34] Migahed M D, Fahmy T, Ishra M and Baraket A 2004 *Polym. Test.* **23** 361–5
[35] Holland E R, Pomfret S J, Admas P N and Monkman A P 1996 *J. Phys.: Condens. Matter* **8** 2991–3002
[36] Sakkopoulos S, Vitoratos E and Dalas E 1998 *Synth. Met.* **92** 63–7
[37] Sheng P 1990 *Phys. Rev.* B **21** 2180–95
[38] Sheng P and Abeles B 1973 *Phys. Rev. Lett.* **31** 44
[39] Suri K, Annapoorni S and Tandon R P 2003 *J. Non-Cryst. Solids* **332** 279–85
[40] Dutta P, Biswas S and De S K 2001 *J. Phys.: Condens. Matter* **13** 9187–96
[41] Papathanassiou A N 2002 *J. Phys. D: Appl. Phys.* **35** L88–9
[42] Long A R 1982 *Adv. Phys.* **31** 553–637
[43] Dyre J C and Schroder T B 2000 *Rev. Mod. Phys.* **72** 873
[44] Long A R and Balkan N 1980 *J. Non-Cryst. Solids* **35/36** 415–20
[45] Okutan M, Basaran E, Bakan H I and Yakuphanoglu F 2005 *Physica* B **364** 300–5

[46] Elliott S R 1977 *Phil. Mag.* **36** 1291–304
[47] Pinto N J, Torres C M, Kahol P K and McCormik B J 1996 *J. Appl. Phys.* **79** 8512
[48] Fattoum A, Arous M, Gmati F, Dhaoui W and Mohamed A B 2007 *J. Phys. D: Appl. Phys.* **40** 4347–54
[49] Ohsawa T, Kabata T and Kimura O 1989 *Synth. Met.* **29** E203–10
[50] Bajer I K, Zagorska M, Niziol J, Pron A and Luzny E 2000 *Synth. Met.* **114** 125–31
[51] Wu Q, Xue Z, Qi Z and Wang F 2000 *Polymer* **41** 2029–32
[52] Ahrony A and Stauffer D 1993 *Introduction to Percolation Theory* 2nd edn (London: Taylor and Francis)
[53] Sharma J P and Sekhon S S 2006 *Mater. Sci. Eng.* B **129** 104–8
[54] Singh R, Arora V, Tandan R P and Chandra S 1998 *J. Mater. Sci.* **33** 2067–72
[55] Cappacioli S, Lucchesi M, Rolla P A and Ruggeri G 1998 *J. Phys.: Condens. Matter* **10** 5595–617
[56] Alig I, Dudkin S M, Jenninger W and Marzantowicz M 2006 *Polymer* **47** 1722–31
[57] Papathanassiou A N, Sakellis I, Grammatikakis J, Vitoratos E, Sakkopooulos S and Dalas E 2004 *Synth. Met.* **142** 81–4
[58] Psarras G C 2006 *Composite* A **37** 1545–53
[59] Jonscher A K 1983 *Dielectric Relaxation in Solids* (London: Chelsea Dielectric Press) chapter 3, p 39